Diagnosing destabilisation risk in global land carbon sinks

Authors: Marcos Fernández-Martínez[1,2,3], Josep Peñuelas[2,4], Frederic Chevallier[5], Philippe Ciais[5], Michael Obersteiner[6,7], Christian Rödenbeck[8], Jordi Sardans[2,4], Sara Vicca[1], Hui Yang[5], Stephen Sitch[9], Pierre Friedlingstein[10], Vivek K. Arora[11], Daniel S. Goll[5], Atul K. Jain[12], Danica L. Lombardozzi[13], Patrick C. McGuire[14], Ivan A. Janssens[1].

Affiliations:

[1] PLECO (Plants and Ecosystems), Department of Biology, University of Antwerp, 2610 Wilrijk, Belgium.

[2] CREAF, E08193 Bellaterra (Cerdanyola del Vallès), Catalonia, Spain

[3] BEECA-UB, Department of Evolutionary Biology, Ecology and Environmental Sciences, University of Barcelona, E08028 Barcelona, Catalonia, Spain

[4] CSIC, Global Ecology Unit, CREAF-CSIC-UAB, Bellaterra, 08193 Barcelona, Catalonia, Spain

[5] Laboratoire des Sciences du Climat et de l'Environnement, LSCE/IPSL, CEA-CNRS-UVSQ, Université Paris-Saclay, Gif-sur-Yvette, France

[6] International Institute for Applied Systems Analysis (IIASA), Laxenburg, Austria

[7] School of Geography and the Environment, University of Oxford, Oxford, UK

[8] Department of Biogeochmical Systems, Max Planck Institute for Biogeochemistry, Jena, Germany

[9] College of Life and Environmental Sciences, University of Exeter, Exeter, UK

[10] College of Engineering, Mathematics, and Physical Sciences, University of Exeter, Exeter, United Kingdom

[11] Canadian Centre for Climate Modelling and Analysis, Climate Research Division, Environment and Climate Change Canada, Victoria, BC, Canada

[12] Department of Atmospheric Sciences, University of Illinois, Urbana, IL 61801, USA

[13] Climate and Global Dynamics Laboratory, National Center for Atmospheric Research, Boulder, CO 80302, United States of America

[14] Department of Meteorology, Department of Geography & Environmental Science, National Centre for Atmospheric Science, University of Reading, Reading, UK

*__Correspondence to__: M. Fernández-Martínez, m.fernandez@creaf.uab.cat

Length of the main text: 3176 words

Figures and tables: 3 figures, 0 tables

References: 46 (+ 14 in Methods)

Summary

Global net land carbon uptake, or net biome production (NBP), has increased during recent decades[1]. Whether its temporal variability and autocorrelation have changed during this period, however, remains elusive, even though an increase in both could indicate an increased potential for a destabilised carbon sink[2,3]. Here we investigate the trends and controls of net terrestrial carbon uptake and its temporal variability and autocorrelation from 1981 to 2018 using two atmospheric inversion models, the amplitude of the seasonal cycle of atmospheric CO_2 concentration derived from nine monitoring stations distributed across the Pacific Ocean and dynamic global vegetation models. We find that annual NBP and its interdecadal variability increased globally while temporal autocorrelation decreased. We observe a separation of regions characterized by increasingly variable NBP, associated with warm regions and increasingly variable temperatures, lower and weaker trends in NBP, and regions where NBP became stronger and less variable. Plant species richness presented a concave-down parabolic spatial relationship with NBP and its variability at the global scale while nitrogen deposition generally increased NBP. Increasing temperature and its increasing variability appears as the most important drivers of declining and increasingly variable NBP. Our results show increasing variability of NBP regionally that can be mostly attributed to climate change, and that may point to destabilisation of the coupled carbon-climate system.

Keywords: carbon cycle, variability, biodiversity, climate, land-use change, early warnings

Main

Positive carbon-climate feedbacks have the potential to accelerate climate change and might compromise the attainability of ambitious climate targets such as those set by the Paris agreement[4]. Terrestrial ecosystems are key to the functioning of the global carbon (C) cycle and have increased their productivity and net C uptake during recent decades primarily due to CO_2 fertilisation and forest regrowth[1,5–7]. However, land-use change, nutrient limitations and increasing droughts and fires are constraining this potential to sequester C[8–11]. Identifying processes that might destabilise net land C uptake (or net biome production, NBP) is of paramount importance for understanding and managing the global C cycle.

Destabilisation is the process of losing stability: that is, when a system loses its ability to return to equilibrium following a disturbance. A symptom of this may be increased variability, as the system spirals away from its current equilibrium point towards a new one. Destabilisation of a dynamical system is usually accompanied by concomitant increases in temporal variability and autocorrelation (i.e., the correlation between consecutive time steps [AR1] also related to reduced resilience[2]) when AR1 is already positive, because anomalous states of the system create ripples that can get amplified through time rather than compensated as when AR1 is negative. Consequently, increasing temporal variability and autocorrelation have been shown to be potential early-warning signals for abrupt shifts in ecosystems[2,3,12,13]. To date, changes in NBP temporal variability and autocorrelation have not yet been investigated even though increased stress and changes in the frequency and intensity of extreme weather events are likely to alter the temporal patterns of NBP[14–16] due to *i*) a cumulative negative effect of extreme events on ecosystem functioning, *ii*) increasing climate variability and, *iii*) decreasing ecosystem resilience due to increased stress. We, thus, hypothesised that regions experiencing increasing trends in climate variability will also experience increasing variability in their NBP, and that increase in variability may indicate that a destabilisation of the net land C uptake is occurring. This finding could serve as an early warning signal for abrupt shifts in ecosystem's functions[2] that might lead to regime shifts in the Earth's biosphere[17,18]. Even if these changes do not occur at the global scale, increasing temporal variability and autocorrelation in several regions of the globe (e.g. Amazon basin, boreal ecosystems with permafrost) could have a profound impact on the global C balance and a knock-on effect on other ecosystem functions.

Climate is the primary control on NBP in terrestrial ecosystems worldwide in space and time[19,20], together with soil nutrient availability[10,21], atmospheric nitrogen (N) deposition, land use and management, and increasing atmospheric CO_2[1]. Generally, gross C fluxes (such as photosynthesis and respiration) are larger in the tropics where high temperature coincides with

sufficient precipitation to enable long growing seasons. However, net C uptake tends to be higher in temperate regions due to higher nutrient availability[19,21–23]. Nutrient availability and N deposition have indeed been shown to increase net land C uptake[21,22]. Another factor believed to be important in determining ecosystem functioning is plant biodiversity[24]. A large body of evidence indicates its role in promoting ecosystem productivity and stability[25,26]. Plant biodiversity, however, has been included far less in studies of ecosystem C cycling, presumably due to the difficulty of acquiring good data on species diversity. The few studies that included biodiversity, however, showed relatively modest correlations with C fluxes[27–29]. The role of biodiversity in the global terrestrial NBP has not yet been explored even though the Earth's biosphere is losing biodiversity at an unprecedented speed[30] and those changes are expected to alter ecosystem functioning.

The aim of this study was to quantify the trends in global NBP and its intradecadal temporal variability (quantified by the proportional variability index, PV[31,32]) and autocorrelation (AR1) to see whether changes in these variables suggest that NBP at global or regional scales is being destabilised. We further tested whether regions with increasing variability and AR1 in NBP showed differential trends in annual NBP. We additionally investigated the spatial correlation between NBP metrics and plant biodiversity (derived from a global map of plant species richness[33]), atmospheric total N deposition[34], climate[35], and land use (land-use harmonisation[2] maps). To realise these objectives, we used estimates of NBP derived from the two longest CO_2 atmospheric inversions (CAMS, CarboScope) and the amplitude of the seasonal cycle of atmospheric CO_2 derived from nine monitoring stations distributed from south to north of the Pacific Ocean for 1981 to 2018. We additionally compared these results with the output from an ensemble of 12 dynamic global vegetation models (TRENDY) to explore how well these state-of-the-art models predict the spatial and temporal patterns in NBP simulated by atmospheric inversion models.

Results

Temporal patterns of net land C uptake

Global NBP derived from atmospheric inversions increased from 5.6 ± 2.0 gC m^{-2} y^{-1} during 1981 – 1990 (mean ± standard error) to 13.8 ± 1.4 gC m^{-2} y^{-1} during 2009 – 2018 over the global land area excluding Antarctica (**Figure 1**). This represents an overall increase of 145% and an annual linear increase of 0.24 ± 0.08 gC m^{-2} y^{-2} (P<0.001). Both atmospheric inversions used (CAMS and CarboScope) identified annual increases in NBP (**Supplementary Figure 1** and **Supplementary Figure 2**, 0.32 ± 0.09, and 0.18 ± 0.09 gC m^{-2} y^{-2} respectively, P<0.001, N=38). The positive trend in NBP shown by inversions is similar in magnitude to the trend identified by the TRENDY ensemble (0.10 ± 0.07 gC m^{-2} y^{-2}, P<0.001; 147% when comparing

the periods 1981 – 1990 and 2009 – 2018). Both observations and models, however, showed a flattening trend during the last decade (**Figure 1c**). In parallel with the increased NBP throughout the entire study period and in agreement with previous literature[36,37], the amplitude of the seasonal atmospheric CO_2 concentration increased by 0.027 ± 0.004 ppm y^{-1} (P<0.001, 16.6% during the study period) (**Supplementary Figure 3a**).

Interannual NBP variability (NBP_{PV}) derived from the combination of atmospheric inversions increased globally by 7.2% over the entire period (P<0.001) (**Figure 1f**) (CAMS 14.9%, P<0.001; CarboScope: -1.3%, P<0.001). The origin of the discrepancy between the inversions remains unclear. Though the inversions differ in whether they use a growing number of measurement stations (CAMS) or a constant station set (CarboScope), the discrepancy is unlikely to be related to this because a test inversion with a growing station set in the CarboScope inversion did not yield an increase in NBP_{PV}. Temporal variability in the amplitude of the seasonal atmospheric CO_2 concentration also increased (by 35%, P<0.001) during the study period (**Supplementary Figure 3b**). TRENDY NBP did not simulate this increase in variability, showing a negative trend of -1.7% in NBP_{PV} similar to that from the CarboScope inversion.

Global NBP_{AR1} significantly decreased over time for NBP derived from atmospheric inversions (**Figure 1i**) and for the average monthly CO_2 concentrations across the Pacific Ocean (**Supplementary Figure 3c**). TRENDY NBP_{AR1}, also showed a significant negative trend representing a reduction of 2.9% over the study period. Trends of contrasting sign, however, were significant amongst atmospheric measurement stations and atmospheric inversions (CAMS: -10.0%, P<0.001; CarboScope: 4.7%, P<0.001). Several regions showed increases in the temporal autocorrelation between consecutive months (NBP_{AR1}) derived from atmospheric inversions that are of a similar magnitude (ca. 0.2 over three decades) to those previously suggested to precede abrupt shifts in climate datasets and simulations[2,3]. Additional information on how changes in NBP_{PV} and NBP_{AR1} may affect annual NBP and their limitations can be found in Supplementary text, Section 1.

Our analyses identified several regions of potential concern given their concomitant increase in NBP_{PV} and NBP_{AR1} (**Figure 2a**), such as eastern Africa, the Mediterranean region, the west coasts of North and Central America, India, and southeast Asia. Regions with increasing NBP_{PV} and NBP_{AR1} had statistically lower NBP and experienced a much less pronounced increase in NBP over time (0.15 ± 0.06 gC m^{-2} y^{-1}, P<0.001) compared to regions where NBP_{PV} and NBP_{AR1} decreased (0.73 ± 0.12 gC m^{-2} y^{-1}, P<0.001) (**Figure 2b-d, Supplementary Figure 4**). Stronger increases in NBP over regions with decreasing NBP_{PV} and NBP_{AR1},

compared to those where they increased, were also evident from both atmospheric inversions when analysed separately (**Supplementary Figure 5**).

Global temperature and precipitation increased during the study period (**Supplementary Figure 6a and d**) even though there was considerable spatial variability in those trends (**Supplementary Figure 7a and d**). Temperature and precipitation interannual variability, however, decreased significantly at the global scale, despite the reported increase in extreme weather[14]. Temporal autocorrelation of monthly temperature and precipitation, instead, increased slightly, albeit only significantly for temperature. A concomitant increase in temporal variability and autocorrelation of temperature was evident in several regions (e.g., Eurasia, Australia, Central America) but those were not so obvious for precipitation (**Supplementary Figure 8**).

Controls of NBP, variability and autocorrelation

NBP, derived from atmospheric inversions, had a concave-down parabolic relationship with biodiversity **(Figure 3)**, increasing from low to intermediate values of biodiversity and decreasing at high biodiversity (**Supplementary Figure 9a**). Our analyses also identified a significant positive interaction between biodiversity and N deposition accounting for NBP. The concave-down relationship between biodiversity and NBP included mainly positive NBP values across regions with high atmospheric N deposition (850 mg N m^{-2} y^{-1}) and mainly negative NBP values at low atmospheric N deposition (100 mg N m^{-2} y^{-1}) (**Supplementary Figure 9a**). Similarly, the positive correlation between N deposition and NBP was stronger in regions with higher plant biodiversity (**Supplementary Figure 9b**). Opposite relationships emerged when analysing TRENDY NBP.

NBP_{PV} derived from inversions also showed a concave-down parabolic relationship with plant biodiversity, peaking at intermediate to high values of biodiversity (**Supplementary Figure 9d**). We also found an interaction between plant biodiversity and N deposition in their relationship with NBP_{PV}: the relationship between NBP_{PV} and biodiversity differed between areas receiving low N deposition and areas receiving high N deposition (**Supplementary Figure 9d**). No relationship between N deposition and NBP_{PV} was found in regions with high biodiversity, whereas a positive relationship occurred in regions with low biodiversity (**Supplementary Figure 9e**). Interannual variability in temperature and precipitation were positively correlated with NBP_{PV} (**Figure 3**). In this case, the patterns for the TRENDY ensemble and the inversion models matched very well. Again, NBP_{AR1} derived from inversions had a concave-down parabolic relationship with biodiversity (**Supplementary Figure 9g**), but here no interaction occurred between the effects of biodiversity and N deposition, which was negatively correlated with NBP_{AR1}. NBP_{AR1} was also positively correlated with temperature

AR1, the only result that match those from TRENDY NBP_{AR1} (**Supplementary Figure 9i**). Results emerging from individual atmospheric inversions (CAMS and CarboScope) mostly coincided with those reported above (**Supplementary Figure 10**).

Spatial variability in the trends of NBP, NBP_{PV} and NBP_{AR1} derived from atmospheric inversions were all correlated with N deposition, climate, and land use (**Figure 3** and **Supplementary Figure 11**). The estimated effects of land use and land use change, however, were generally lower than those from N deposition and climate, hence accounting for a smaller proportion of the change at the global scale. N deposition was positively correlated with the trends in NBP and negatively with trends in NBP_{PV} and NBP_{AR1} **(Supplementary Figure 11)**. Warmer regions were more likely than colder regions to have decreasing trends in NBP, and increasing temperatures contributed to decreasing NBP (**Supplementary Figure 11b and c**). Regions with the strongest increases in NBP_{PV} were spatially associated with low increases in annual temperature (**Supplementary Figure 11e**). Increases in NBP_{PV} were also found to be more likely in regions showing increases in temperature temporal variability (**Supplementary Figure 11f**). Increasing NBP_{AR1} was more likely in regions with increasing temperatures (**Supplementary Figure 11h**) and mildly with increasing temporal autocorrelation of precipitation (**Figure 3**). Our analyses using TRENDY reproduced the abovementioned findings well for trends in NBP and NBP_{AR1}, but not for NBP_{PV}. Again, results from individual atmospheric inversions were very similar to those reported here (**Supplementary Figure 10**). Warm regions presenting a concomitant increase in temperature temporal variability and autocorrelation (symptoms of destabilisation) were more likely to be correlated with similar changes in NBP variability and AR1, and those results were well supported by both atmospheric inversions and their combination (**Supplementary Figure 12**). Additionally, regions with higher N deposition, larger proportions of forested areas and lower crops were related to concomitantly decreasing NBP_{PV} and NBP_{AR1}.

Biodiversity, N deposition and net C uptake

NBP derived from atmospheric inversions provided correlational evidence indicating that plant biodiversity may be playing an important role in regulating regional variation in the land C balance and in its temporal variability. TRENDY models, instead, do not include biodiversity in their parameterisation and, hence, any spurious relationship is necessarily driven by factors other than biodiversity. The spatial relationship between biodiversity and NBP clearly differed between atmospheric inversions and TRENDY (**Supplementary Figure 9a**), hence suggesting that the reported effect of biodiversity when analysing atmospheric inversions may emerge due to a mechanistic effect. The emerging relationship between biodiversity and NBP_{PV} derived from atmospheric inversions, however, was very similar to the one emerging

from TRENDY, which suggests that factors other than biodiversity may be driving this relationship. The positive relationship between biodiversity and NBP_{AR1} found here has never been reported before and further research is needed to understand the mechanisms behind this relationship.

The concave-down parabolic relationships of biodiversity with NBP and NBP_{PV} differ from the majority of biodiversity-productivity and stability relationships reported in the literature: positive asymptotic for productivity and negative for variability[38,39]. This difference in the biodiversity-NBP relationship may result from two opposing ecosystem processes, photosynthesis and respiration, because both are likely to be enhanced by biodiversity[27,40,41]. The concave-down relationship would then suggest that the positive effect of biodiversity on respiration overshadows the positive effect of photosynthesis in regions with high biodiversity. However, our biodiversity data, like in similar studies[39], was restricted to species richness and did not include information on species abundance, their individual contribution to NBP, or traits to allow the calculation of actual species diversity or functional diversity, often better indicators of ecosystem functioning than species richness[42]. Unfortunately, this information is not available at the global scale. Including actual diversity in future analyses could lead to different results to those reported here. Additionally, future efforts are needed to understand how biodiversity loss, not included here, will impact global carbon balance.

Interestingly, our analyses indicated that the effect of biodiversity on NBP depended on atmospheric N deposition, and vice versa (**Figure 3**). The effect of atmospheric N deposition on NBP was mainly positive but was stronger in regions with higher biodiversity, further supporting the premise that biodiversity promotes ecosystem functions such as N uptake[43]. Regions with higher N deposition also had larger increases in NBP over time (**Supplementary Figure 11a**), supporting previous findings suggesting a stronger CO_2 fertilisation effect in regions with higher N deposition[1]. On the other hand, N deposition was negatively related to trends in NBP_{PV}, NBP_{AR1} and the aggregated trend of $NBP_{PV\text{-}AR1}$ (**Supplementary Figure 12**), which suggests that N addition may ameliorate nutrient imbalances derived from increasing atmospheric CO_2 concentrations[8] and prevent ecosystem functioning from becoming more variable.

Climate and changing land C uptake

Our results clearly indicate that NBP decreased in regions with warm climates and where warming has been most pronounced (**Supplementary Figure 11**). These findings support results from previous studies[1] and further suggests that increasing droughts and heat waves limit C sequestration by terrestrial ecosystems[44]. Our analyses revealed that higher NBP_{PV}, NBP_{AR1} and their trends were associated, respectively, with climates showing higher and

increasing temporal variability and autocorrelation (**Supplementary Figure 9**). We also found that concomitantly increasing trends in $NBP_{PV\text{-}AR1}$ were positively related to increasing temperature variability and autocorrelation (**Supplementary Figure 12**). These results support our initial hypothesis stating that climate change may be the main contributing factor for changing the temporal behaviour of land C sinks.

Implications of altered land C sinks

Compelling evidence from atmospheric inversions (**Figure 1**) and the annual amplitude of the seasonal CO_2 cycle (**Supplementary Figure 3**) suggests that global net land C uptake is now larger and, most likely, more variable than three decades ago, while its temporal autocorrelation (NBP_{AR1}), instead, has significantly decreased. The increase in global NBP and the reduction in NBP_{AR1} were well identified by TRENDY NBP, including the evidence of a flattening trend in NBP during the last two decades. Our results for the increase in global NBP and a potential recent saturation are consistent with previous findings of increases in global productivity and NBP and a recent decline of the CO_2 fertilisation effect[1,5,8,20]. Even though the main emerging spatial controls for CAMS and CarboScope atmospheric inversions in NBP were in agreement (**Figures S8** and **S10**), trends at the global scale for NBP_{PV} and NBP_{AR1} were significantly different (**Supplementary Figure 13**), which calls for caution in the interpretation of these results due to their uncertainty.

We observed a bifurcation of regions characterised by concomitant increases and decreases in NBP_{PV} and NBP_{AR1} **(Figure 2)**. This bifurcation relates to differences in their mean annual temperature, their increase in annual temperature, their average N deposition loads and their percentage of forests and crops (**Supplementary Figure 12**). The observed increase in the variability and autocorrelation of net C uptake in several regions of the planet (**Figure 2a**) is concerning because of the implications it can have on the stability of their ecosystems. First, increasing NBP_{PV} and NBP_{AR1} is indicative of increasing variability and reducing resilience[3,45] potentially in many ecosystem processes: from photosynthesis and respiration[27] to cascading effects on animals and decomposers[46]. Second, an increase in variability in NBP implies that ecosystem C balance is less predictable over time, which is troublesome for projections of future climate change. Third, regions showing a combined increase in NBP_{PV} and NBP_{AR1} had a consistently lower NBP and lower increases in NBP than regions where NBP_{PV} and NBP_{AR1} decreased (**Figure 2b-d**), suggesting that these increases NBP_{PV} and NBP_{AR1} reflect dynamical instability in the carbon system rather than some other cause (such as changes in the external forcing of the system). This destabilization may jeopardise future C sequestration. Our analyses, however, could not determine the mechanisms driving the observed changes in NBP_{PV} and NBP_{AR1}. More importantly, we could not determine whether the observed increases

NBP_{PV} and NBP_{AR1} truly reflect dynamical instability in the carbon system, as opposed to some other cause, such as changes in the external forcing of the system (e.g., increasing CO_2 emissions, N deposition). Hence, regions showing increased variability and autocorrelation should be monitored in detail to properly understand the mechanisms and consequences behind these changes given that increasing variability and autocorrelation have been shown to act as early warning signals preceding abrupt phase transitions in simulations of ecosystem functioning[2,3]. The increase of NBP_{PV} and NBP_{AR1} in several regions should serve as an early warning signal of potential future changes that the Earth's biosphere may be facing. Given the main role of climate change as a driver of these changes in their temporal behaviour, mitigating climate change is needed to prevent further unforeseen changes in land C sinks.

References

1. Fernández-Martínez, M. *et al.* Global trends in carbon sinks and their relationships with CO2 and temperature. *Nat. Clim. Chang.* **9**, 73–79 (2019).

2. Scheffer, M. *et al.* Early-warning signals for critical transitions. *Nature* **461**, 53–59 (2009).

3. Dakos, V. *et al.* Slowing down as an early warning signal for abrupt climate change. *Proc. Natl. Acad. Sci. U. S. A.* **105**, 14308–14312 (2008).

4. Gasser, T. *et al.* Path-dependent reductions in CO2 emission budgets caused by permafrost carbon release. *Nat. Geosci.* **11**, 830–835 (2018).

5. Zhu, Z. *et al.* Greening of the Earth and its drivers. *Nat. Clim. Chang.* **6**, 791–795 (2016).

6. Bastos, A. *et al.* Contrasting effects of CO2 fertilization, land-use change and warming on seasonal amplitude of Northern Hemisphere CO2 exchange. *Atmos. Chem. Phys.* **19**, 12361–12375 (2019).

7. Pugh, T. A. M. *et al.* Role of forest regrowth in global carbon sink dynamics. *Proc. Natl. Acad. Sci. U. S. A.* **116**, 4382–4387 (2019).

8. Wang, S. *et al.* Recent global decline of CO2 fertilization effects on vegetation photosynthesis. *Science (80-.).* **370**, 1295–1300 (2020).

9. Peñuelas, J. *et al.* Assessment of the impacts of climate change on Mediterranean terrestrial ecosystems based on data from field experiments and long-term monitored field gradients in Catalonia. *Environ. Exp. Bot.* (2017)

doi:10.1016/j.envexpbot.2017.05.012.

10. Terrer, C. *et al.* Nitrogen and phosphorus constrain the CO2 fertilization of global plant biomass. *Nat. Clim. Chang.* (2019) doi:10.1038/s41558-019-0545-2.

11. Gatti, L. V. *et al.* Amazonia as a carbon source linked to deforestation and climate change. *Nature* **595**, 388–393 (2021).

12. Carpenter, S. R. & Brock, W. A. Rising variance: A leading indicator of ecological transition. *Ecol. Lett.* **9**, 311–318 (2006).

13. Dakos, V., Nes, E. H. & Scheffer, M. Flickering as an early warning signal. *Theor. Ecol.* **6**, 309–317 (2013).

14. Sillmann, J., Daloz, A. S., Schaller, N. & Schwingshackl, C. *Extreme weather and climate change*. *Climate Change* (Elsevier B.V., 2021). doi:10.1016/b978-0-12-821575-3.00016-5.

15. Reichstein, M. *et al.* Climate extremes and the carbon cycle. *Nature* **500**, 287–95 (2013).

16. Wang, X. *et al.* A two-fold increase of carbon cycle sensitivity to tropical temperature variations. *Nature* **506**, 212–5 (2014).

17. Barnosky, A. D. *et al.* Approaching a state shift in Earth's biosphere. *Nature* **486**, 52–8 (2012).

18. Buermann, W. *et al.* Climate-driven shifts in continental net primary production implicated as a driver of a recent abrupt increase in the land carbon sink. *Biogeosciences* **13**, 1597–1607 (2016).

19. Luyssaert, S. *et al.* CO 2 balance of boreal, temperate, and tropical forests derived from a global database. *Glob. Chang. Biol.* **13**, 2509–2537 (2007).

20. Peñuelas, J. *et al.* Shifting from a fertilization-dominated to a warming dominated period. *Nat. Ecol. Evol.* **1**, 1438–1445 (2017).

21. Fernández-Martínez, M. *et al.* Nutrient availability as the key regulator of global forest carbon balance. *Nat. Clim. Chang.* **4**, 471–476 (2014).

22. Fernández-Martínez, M. *et al.* Spatial variability and controls over biomass stocks, carbon fluxes and resource-use efficiencies in forest ecosystems. *Trees, Struct. Funct.* **28**, 597–611 (2014).

23. Ciais, P. *et al.* Five decades of northern land carbon uptake revealed by the interhemispheric CO2 gradient. *Nature* **568**, 221–225 (2019).

24. Tilman, D., Lehman, C. L. & Thomson, K. T. Plant diversity and ecosystem productivity: Theoretical considerations. *Proc. Natl. Acad. Sci.* **94**, 1857–1861 (1997).

25. de Mazancourt, C. *et al.* Predicting ecosystem stability from community composition and biodiversity. *Ecol. Lett.* **16**, 617–625 (2013).

26. Sakschewski, B. *et al.* Resilience of Amazon forests emerges from plant trait diversity. *Nat. Clim. Chang.* **6**, 1032–1036 (2016).

27. Fernández-Martínez, M. *et al.* The role of climate, foliar stoichiometry and plant diversity on ecosystem carbon balance. *Glob. Chang. Biol.* **26**, 7067–7078 (2020).

28. Musavi, T. *et al.* Stand age and species richness dampen interannual variation of ecosystem-level photosynthetic capacity. *Nat. Ecol. Evol.* **1**, 0048 (2017).

29. Anderegg, W. R. L. *et al.* Hydraulic diversity of forests regulates ecosystem resilience during drought. *Nature* **561**, 538–541 (2018).

30. Díaz, S. *et al. IPBES, 2019. Summary for policymakers of the global assessment report on biodiversity and ecosystem services of the Intergovernmental Science-Policy Platform on Biodiversity and Ecosystem Services*. (2019) doi:10.1111/padr.12283.

31. Heath, J. P. Quantifying temporal variability in population abundances. *Oikos* **115**, 573–581 (2006).

32. Fernández-Martínez, M., Vicca, S., Janssens, I. A., Martín-Vide, J. & Peñuelas, J. The consecutive disparity index, D, as measure of temporal variability in ecological studies. *Ecosphere* **9**, e02527 (2018).

33. Kreft, H. & Jetz, W. Global patterns and determinants of vascular plant diversity. *Proc Natl Acad Sci U S A* **104**, 5925–5930 (2007).

34. Ackerman, D. E., Chen, X. & Millet, D. B. Global nitrogen deposition (2°×2.5° grid resolution) simulated with GEOS-Chem for 1984-1986, 1994-1996, 2004-2006, and 2014-2016. (2018) doi:10.13020/D6KX2R.

35. Harris, I., Jones, P. D. D., Osborn, T. J. J. & Lister, D. H. H. Updated high-resolution grids of monthly climatic observations - the CRU TS3.10 Dataset. *Int. J. Climatol.* **34**, 623 – 642 (2013).

36. Graven, H. D. *et al.* Enhanced seasonal exchange of CO2 by northern ecosystems since 1960. *Science* **341**, 1085–9 (2013).

37. Wang, K. *et al.* Causes of slowing-down seasonal CO2 amplitude at Mauna Loa. *Glob. Chang. Biol.* **26**, 4462–4477 (2020).

38. Tilman, D., Reich, P. B. & Knops, J. M. H. Biodiversity and ecosystem stability in a decade-long grassland experiment. *Nature* **441**, 629–32 (2006).

39. Liang, J. *et al.* Positive biodiversity-productivity relationship predominant in global forests. *Science (80-.).* **354**, aaf8957–aaf8957 (2016).

40. Gessner, M. O. *et al.* Diversity meets decomposition. *Trends Ecol. Evol.* **25**, 372–380 (2010).

41. Peguero, G. *et al.* Fast attrition of springtail communities by experimental drought and richness–decomposition relationships across Europe. *Glob. Chang. Biol.* **25**, 2727–2738 (2019).

42. Díaz, S. & Cabido, M. Vive la différence: Plant functional diversity matters to ecosystem processes. *Trends Ecol. Evol.* **16**, 646–655 (2001).

43. Cardinale, B. J. Biodiversity improves water quality through niche partitioning. *Nature* **472**, 86–91 (2011).

44. Ciais, P. *et al.* Europe-wide reduction in primary productivity caused by the heat and drought in 2003. *Nature* **437**, 529–533 (2005).

45. Scheffer, M. *Critical Transitions in Nature and Society*. (Princeton University Press, 2009).

46. Ostfeld, R. & Keesing, F. Pulsed resources and community dynamics of consumers in terrestrial ecosystems. *Trends Ecol. Evol.* **15**, 232–237 (2000).

Figure 1: Global distribution of net biome production (NBP), its interannual variability (NBP_{PV}) and temporal autocorrelation (NBP_{AR1}), and their trends from 1981 to 2018. Panel a shows the average global distribution of NBP (positive values indicate C sinks) derived from CAMS and CarboScope atmospheric inversions. Panel b shows the temporal trends in NBP (∆NBP), and panel c shows the temporal change in NBP derived from atmospheric inversions and 12 DGVMs (TRENDY). Panels d, e, and f, and g, h, and i mimic panels a, b, and c, respectively, for interannual variability of NBP (NBP_{PV}) and temporal autocorrelation (NBP_{AR1}) calculated over an 11-year moving window. Thick lines in panels c, f, and i represent smooth trends estimated with a local regression (shaded areas show the standard error of the trend), and the coefficients at the top of the panels indicate robust Theil-Sen's slopes (± standard error of the slope) with their corresponding p-values, estimated using the non-parametric Wilcoxon Mann-Whitney rank sum test. Values in panels c, f and i, represent spatially-weighted global means. **, $P<0.01$; ***, $P<0.001$. Data to reproduce this figure can be found in Source Data 1.

(See **Figure 1** on the following page)

Figure 1

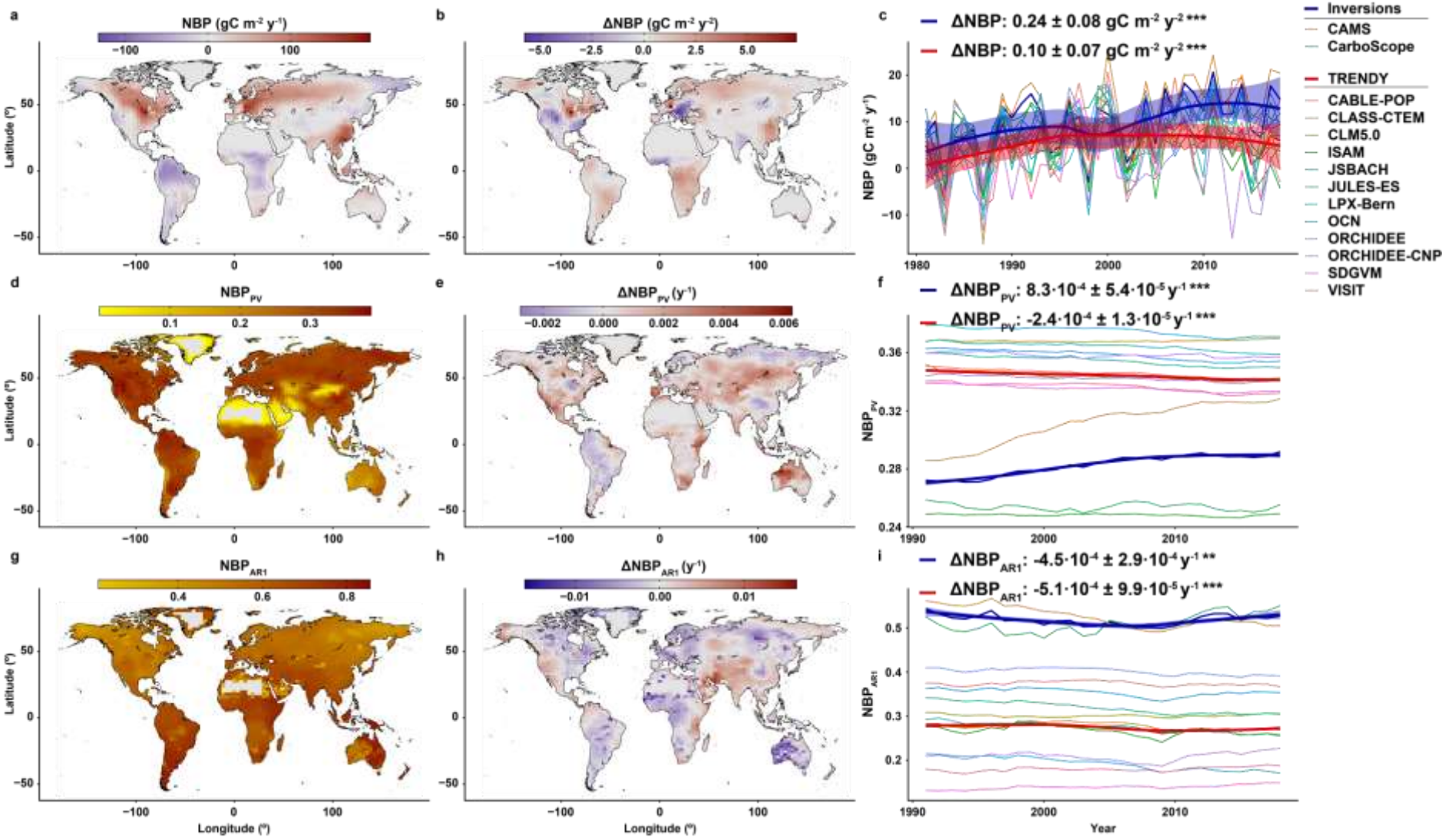
a
NBP (gC m-2 y-1)
−100
0
100
b
ΔNBP (gC m-2 y-2)
−5.0
−2.5
0.0
2.5
5.0
c
ΔNBP: 0.24 ± 0.08 gC m-2 y-2 ***
ΔNBP: 0.10 ± 0.07 gC m-2 y-2 ***
NBP (gC m-2 y-1)
Inversions
CAMS
CarboScope
TRENDY
CABLE-POP
CLASS-CTEM
CLM5.0
ISAM
JSBACH
JULES-ES
LPX-Bern
OCN
ORCHIDEE
ORCHIDEE-CNP
SDGVM
VISIT
d
NBPPV
0.1
0.2
0.3
e
ΔNBPPV (y-1)
−0.002
0.000
0.002
0.004
0.006
f
ΔNBPPV: 8.3·10-4 ± 5.4·10-5 y-1 ***
ΔNBPPV: -2.4·10-4 ± 1.3·10-5 y-1 ***
NBPPV
g
NBPAR1
0.4
0.6
0.8
h
ΔNBPAR1 (y-1)
−0.01
0.00
0.01
i
ΔNBPAR1: -4.5·10-4 ± 2.9·10-4 y-1 **
ΔNBPAR1: -5.1·10-4 ± 9.9·10-5 y-1 ***
NBPAR1
Latitude (°)
Longitude (°)
Year

Figure 2: Regions with concomitantly increasing NBP_{PV} and NBP_{AR1} present lower NBP and a lower increase of NBP over time. Panel a shows regions of the world where concomitant increases (red) and decreases (blue) in NBP_{PV} and NBP_{AR1} have occurred during the study period. Regions with contrasting trends in NBP_{PV} and NBP_{AR1} appear in grey. Panel b shows the aggregated annual mean NBP of regions with increasing (red) and decreasing (blue) NBP_{PV} and NBP_{AR1} (see **Supplementary Figure 4** for information on their global contribution). Smooth trends were estimated with a local regression (shaded indicate the standard error of the trend), and the coefficients at the top of the panel indicate robust Theil-Sen's slopes (± standard error of the slope) and their associated significance (***, *P*<0.001), estimated using the non-parametric Wilcoxon Mann-Whitney rank sum test. Panel c and d show the spatial relationship of NBP and trends in NBP (ΔNBP) with the aggregated trend of NBP_{PV} and NBP_{AR1}. Coefficients are standardised and include the 95% credible intervals (CI). See **Methods** for details on how the aggregated trend of NBP_{PV} and NBP_{AR1} was calculated. Data to reproduce this figure can be found in Source Data 2.

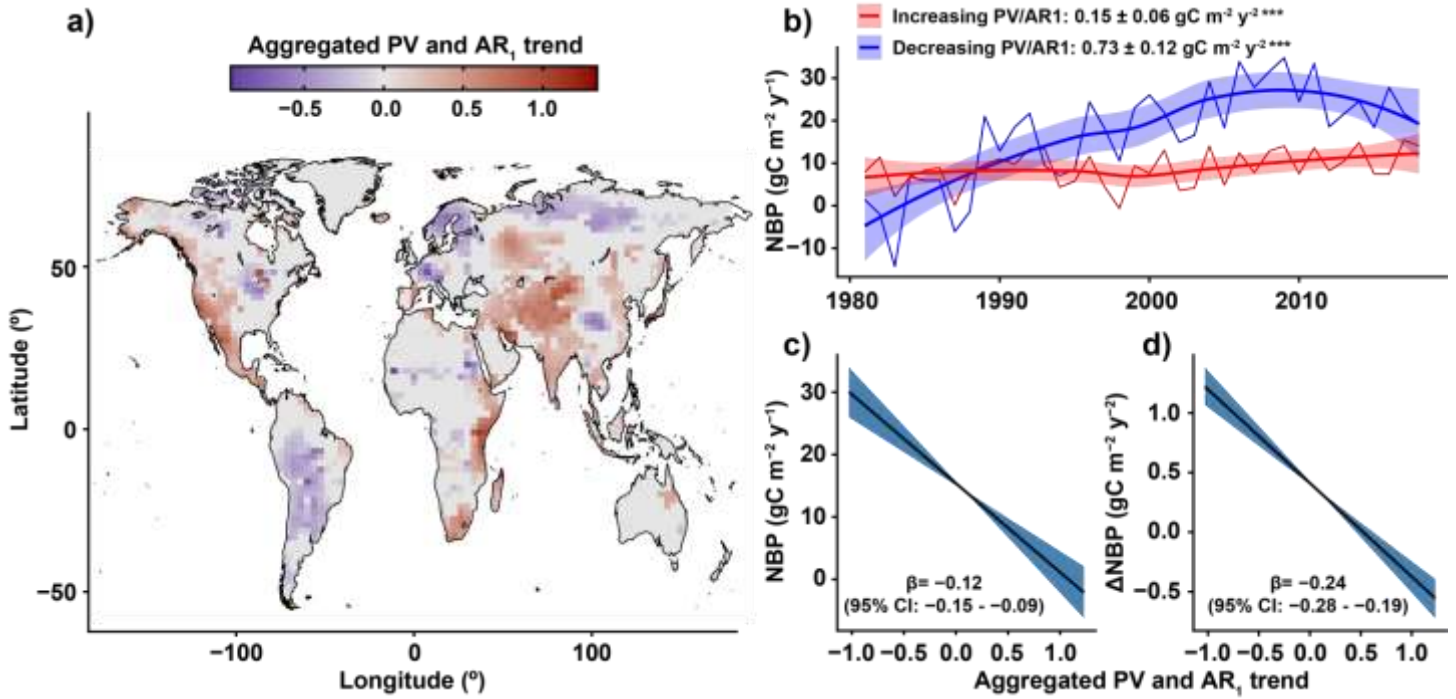

Figure 3: Contribution of biodiversity, N deposition, climate, and land use to the global terrestrial C balance (NBP), its interannual variability (NBP_{PV}), its temporal autocorrelation (NBP_{AR1}), and their trends. The colour scale indicates the strength of the relationship (standardised β coefficients) between each predictor (bottom) and the response variable (left). Black dots indicate that 95% of the posterior distributions differed from 0. Biodiversity was fitted as a second-order polynomial to account for nonlinearities (biodiversity + biodiversity^2; the second term indicates the change in the slope in biodiversity as biodiversity increases). Hashed areas indicate relationships not included in the regression models. See **Methods** for further information on model fitting. INV and TRD indicate the averages for all atmospheric inversions (2) and DGVMs (12), respectively. Predictors $MAT_{\bar{x}, PV, AR1}$ and $MAP_{\bar{x}, PV, AR1}$ indicate mean, PV, or AR1 metrics of MAT and MAP matching the metric of the response variable (e.g. NBP_{INV} ~ $MAT_{\bar{x},}$; $NBP_{PV\text{-}INV}$ ~ MAT_{PV}). The same applies for ΔMAT_{PV}, ΔMAT_{AR1}, $\Delta MAP_{PV,}$ ΔMAP_{AR1}. MAT, mean annual temperature; MAP, mean annual precipitation; PV, proportional variability; AR1, temporal autocorrelation with previous month; Δ, trend in a given variable.

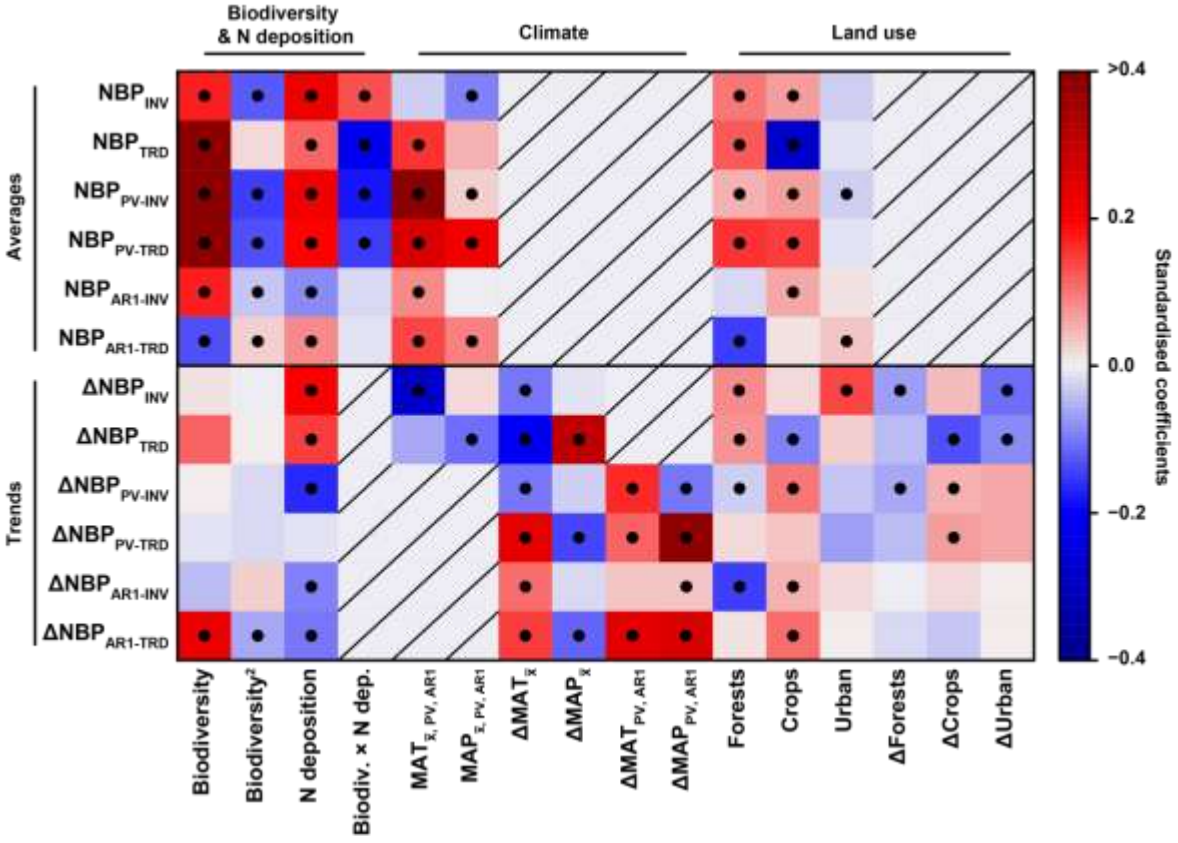

Methods

Data sets

NBP and atmospheric CO_2 data

We obtained the global NBP data for 1981–2018 from the two atmospheric-inversion models that provided the longest time series: i) the CAMS Greenhouse Gases Flux Inversions (https://ads.atmosphere.copernicus.eu/cdsapp#!/dataset/cams-global-greenhouse-gas-inversion)[47,48] version v18r3, and ii) the Jena CarboScope database version s81oc_v2020 using a constant network of measurement stations (http://www.bgc-jena.mpg.de/CarboScope/)[49,50]. We also used NBP data from an ensemble of 12 dynamic global vegetation models (DGVMs) run with varying concentrations of atmospheric CO_2 and changing land uses and climates. Models compiled by the TRENDY project (version 8, models CABLE-POP, CLASS-CTEM, CLM5.0, ISAM, JSBACH, JULES-ES, LPX-BERN, OCN, ORCHIDEE, ORCHIDEE-CNP, SDGVM and VISIT) were used to test whether the DGVMs also identified the patterns from atmospheric inversions[51]. Even though previous studies indicate that DGVMs explain trends in NBP adequately, we are the first to test whether their emerging trends in NBP temporal variability and autocorrelation also match those from local observations or atmospheric inversions. We used model results from the simulation experiment S3, which was run with changing atmospheric CO_2, land use and climate (see https://blogs.exeter.ac.uk/trendy/protocol/ for more details). We used monthly NBP estimates as the basis for all calculations in this study. We rescaled all atmospheric inversions, the TRENDY model outputs, and the predictors to the same spatial resolution of the coarsest data set for fitting the statistical models (see section below) (i.e. CAMS: 3.75 × 1.875°).

We calculated average annual NBP per pixel, its temporal variability expressed as the proportional variability index (NBP_{PV})[31,32], and its monthly temporal autocorrelation at lag 1 (NBP_{AR1}) for all of the abovementioned datasets. All three indices (NBP, NBP_{PV} and NBP_{AR1}) were calculated as the average for the entire period. The PV index is calculated as the mean proportional variability amongst all possible combinations of values in a time series, following: $PV = \frac{2 \sum m}{n(n-1)}$, where "*n*" indicates the length of the variable, where "*m*" is calculated as: $m = 1 - \frac{\min(z_i, z_j)}{\max(z_i, z_j)}$, and where "*z*" represent the individual values from which to calculate all the pairwise comparisons between the observations of the time series (e.g., observation z_i vs observation z_j). When negative values occurred in a time series, we added a constant to the entire time series equivalent to the minimum absolute value plus one.

Unlike other metrics of temporal variability, the PV index provides estimates of temporal variability that are independent of the mean of the time series and that have been proven to be robust even when comparing non-normally distributed data sets, thereby overcoming the mathematical drawbacks of similar variability indices such as the standard deviation or the coefficient of variation[52]. NBP_{PV} per pixel was estimated as the average of the interannual variabilities of all months (e.g. $NBP_{PV} = \frac{NBP_{PV\ January} + [\ldots] + NBP_{PV\ December}}{12}$). By using this method, NBP_{PV} reflects not only the interannual variability of the annual NBP, but also the variation occurring amongst equal months across the years. Using this method, a year with average NBP yet with anomalously low NBP in one period offset by anomalously high NBP in another, would thus result in high interannual variability rather than low interannual variability. AR1 was estimated using the residuals of generalised additive models (GAM) used to remove the trend and seasonal cycle of the data. In these models response variable was monthly NBP and the predictors were the month of the year (i.e. a factor of 12 levels) and the year, the latter included as a spline smoothed term to account for nonlinear trends over time (**Supplementary Figure 14**). We used the *mgcv* R package to fit the GAM models[53]. An 11-year moving average from NBP_{PV} and NBP_{AR1} per pixel was then calculated for all data sets to investigate trends in interannual variability and temporal autocorrelation. Our sensitivity analysis that showed that our results were consistent despite the selection of different window lengths (7, 11 and 15 years, **Supplementary Figure 13, Supplementary Table 1**). Robust Theil-Sen's trends[54] were then calculated for NBP, NBP_{PV} and NBP_{AR1} (ΔNBP, ΔNBP_{PV}, and ΔNBP_{AR1}) per pixel using the *mblm* function in R[55]. Wilcoxon rank sum tests were performed to test the significance of the Theil-Sen's trends. Even though we present results for both atmospheric inversions (CAMS, CarboScope), we combined their results into one fusion dataset in order to further highlight those results for which both inversion models agreed (**Supplementary Figure 10 and Supplementary Figure 12**). The combination was performed by calculating the average value of each of the abovementioned variables per pixel. We followed the same approach to provide a TRENDY dataset combining all simulations following similar studies[1].

Trends in average global NBP, NBP_{PV}, and NBP_{AR1} (from 1981 to 2018 for NBP, from 1991 to 2018 for NBP_{PV}, and NBP_{AR1}) were also estimated using the Theil-Sen's approach. We also combined both atmospheric inversions and the TRENDY simulations to provide the average results derived from atmospheric inversions and process-based models. In this case, the combination of products was performed by calculating the average between products per year and then estimating the temporal trends. We additionally calculated an aggregated metric of trends in NBP_{PV} and NBP_{AR1}. To do so, we first calculated the ratio between each value and the maximum absolute value of each of the variables (ΔNBP_{PV} and

528 ΔNBP_{AR1}) and then we combined them by summing their relative values per pixel. Next, we
529 selected those pixels in which both, ΔNBP_{PV} and ΔNBP_{AR1}, showed a positive trend and
530 those that showed a negative trend, and investigated their respective trends in NBP in the
531 same way that we proceeded for global NBP.

532 Results obtained from the atmospheric inversions were compared with those from nine
533 stations monitoring atmospheric CO_2 concentrations distributed from north to south of the
534 Pacific Ocean that comprised the full period of this study. We selected this subset of
535 monitoring stations to minimise the influence of anthropogenic emissions in the signal of
536 atmospheric CO_2 concentration. These data were downloaded from the Scripps CO_2
537 programme: https://scrippsco2.ucsd.edu/data/atmospheric_co2/[56]. We calculated the
538 annual amplitude in CO_2 concentration (maximum minus minimum) using monthly data
539 following[20,36] as a proxy of the net global C uptake capacity. An 11-year moving average
540 was then used to determine whether the annual amplitude of CO_2 concentrations, its
541 interannual variability (PV), and the monthly temporal autocorrelation (AR1) of CO_2
542 concentrations changed between 1981 and 2018. Theil-Sen slopes were also used to
543 calculate trends in CO_2 amplitude, its interannual variability, and their monthly temporal
544 autocorrelation.

545 *Drivers of NBP*

546 We used temperature and precipitation data from the Climatic Research Unit TS4.03 data
547 set[35] to calculate mean annual temperature (MAT), mean annual precipitation (MAP), their
548 temporal variabilities (MAT_{PV} and MAP_{PV}, average of interannual monthly temporal
549 variability), their monthly temporal autocorrelations (MAT_{AR1} and MAP_{AR1}), as well as the
550 temporal trends of all these metrics (ΔMAT, ΔMAP, ΔMAT_{PV}, ΔMAP_{PV}, ΔMAT_{AR1}, and
551 ΔMAP_{AR1}) for each pixel following the same procedure established for NBP (see above). In
552 order to investigate the controls of the spatial variability in aggregated trends in $NBP_{PV\text{-}AR1}$,
553 we also calculated the aggregated indices for $\Delta MAT_{PV\text{-}AR1}$ and $\Delta MAP_{PV\text{-}AR1}$ following the
554 same methodology used for NBP (see above). Land-use changes were extracted from land-
555 use harmonisation[2] maps (LUH2, http://luh.umd.edu/data.shtml). We calculated the percent
556 coverages of forests, croplands, and urban areas per pixel, and the change in these
557 percentages between 1981 and 2015. We calculated mean total atmospheric N deposition
558 per pixel derived from[34], covering the study period. Biodiversity data were extracted from
559 an interpolated gridded global map of vascular plant biodiversity[33], providing one datum per
560 pixel including information on the current number of vascular plant species. We could not
561 include the effects of biodiversity loss in our analyses because global gridded time series
562 of plant biodiversity are not available.

Statistical analyses

We determined how NBP, NBP_{PV}, NBP_{AR1}, and their trends (ΔNBP, ΔNBP_{PV}, ΔNBP_{AR1} and the combined $\Delta NBP_{PV\text{-}AR1}$) were spatially correlated with their drivers using spatial generalised linear mixed models with a Leroux conditional autoregressive prior[57] and the *S.CARleroux* function in the *CARBayes* R package[58]. All response variables had one datum per pixel, representing aggregated information over the entire study period (e.g., NBP indicates mean annual NBP from 1981 to 2018). Models predicting spatial variability in NBP, NBP_{PV}, and NBP_{AR1} included biodiversity as a second-order polynomial function to account for the nonlinearities usually found between biodiversity and productivity[59] (biodiversity + biodiversity^2), mean atmospheric N deposition, the interaction between biodiversity and N deposition, and the percentages of the area covered by forests and agricultural and urban areas as predictors. MAT and MAP were also included for NBP models, MAT_{PV}, MAP_{PV} for NBP_{PV} models, and MAT_{AR1}, MAP_{AR1} for NBP_{AR1} models. We built an additional model including the interaction between biodiversity and mean and variability in climate (biodiversity:MAT + biodiversity:MAP + biodiversity:MAT_{PV} + biodiversity:MAP_{PV}) and the interactions MAT:MAP and MAT_{PV}:MAP_{PV} to further test that the relationship between NBP and biodiversity was not spuriously emerging due to its relationship with climate (Supplementary information – Model summaries, section 8). As indicated by our results, our analyses were able to successfully discern the effect of biodiversity from that of climate (**Figure 3**). The fact that the relationship between mean NBP and biodiversity emerging from inversions and the TRENDY ensemble (with no parameterisation for biodiversity) were substantially different increases the likelihood of this relationship not being spurious. Models predicting ΔNBP also included the trends in MAT, MAP and the trends in land-use change as predictors. Similarly, models predicting ΔNBP_{PV} and ΔNBP_{AR1} included trends in temperature and precipitation (ΔMAT and ΔMAP) and their temporal variability (ΔMAT_{PV}, ΔMAP_{PV}) or autocorrelation (ΔMAT_{AR1}, ΔMAP_{AR1}) and trends in land-use changes, but not average MAT or MAP or their temporal variability or autocorrelation. Models predicting the combined trends of $\Delta NBP_{PV\text{-}AR1}$ included a second-order biodiversity as a second-order polynomial, N deposition, average and trends in climate, the aggregated trends of $MAT_{PV\text{-}AR1}$ and $MAP_{PV\text{-}AR1}$, average land-use and its temporal trends. We additionally tested whether NBP and ΔNBP were spatially related to increasing $\Delta NBP_{PV\text{-}AR1}$ by fitting two models in which NBP and ΔNBP were the response variables and the aggregated metric of trends in $\Delta NBP_{PV\text{-}AR1}$ (see description above) was their predictor. Models were fitted using normalised variables (mean=0, sd=1), but effect plots were rescaled to their original units to facilitate the interpretation of the results. All analyses were performed using R statistical software v.3.6.3[60].

599

Methods references

47. Chevallier, F. *et al.* CO 2 surface fluxes at grid point scale estimated from a global 21 year reanalysis of atmospheric measurements. *J. Geophys. Res.* **115**, D21307 (2010).

48. Chevallier, F. *et al.* Toward robust and consistent regional CO2 flux estimates from in situ and spaceborne measurements of atmospheric CO2. *Geophys. Res. Lett.* **41**, 1065–1070 (2014).

49. Rödenbeck, C., Houweling, S., Gloor, M. & Heimann, M. CO_2 flux history 1982–2001 inferred from atmospheric data using a global inversion of atmospheric transport. *Atmos. Chem. Phys.* **3**, 1919–1964 (2003).

50. Rödenbeck, C., Zaehle, S., Keeling, R. & Heimann, M. How does the terrestrial carbon exchange respond to interannual climatic variations? A quantification based on atmospheric CO2 data. *Biogeosciences Discuss.* 1–22 (2018) doi:10.5194/bg-2018-34.

51. Sitch, S. *et al.* Recent trends and drivers of regional sources and sinks of carbon dioxide. *Biogeosciences* **12**, 653–679 (2015).

52. Fernández-Martínez, M. & Peñuelas, J. Measuring temporal patterns in ecology: The case of mast seeding. *Ecol. Evol.* **11**, 2990–2996 (2021).

53. Wood, S. N. *Generalized Additive Models: An introduction with R (2nd edition)*. (Chapman and Hall/CRC, 2017). doi:10.1201/9781315370279.

54. Ohlson, J. A. & Kim, S. *Linear valuation without OLS: the Theil-Sen estimation approach*. *Review of Accounting Studies* vol. 20 (2015).

55. Lukasz Komsta. mblm: Median-Based Linear Models. (2013).

56. Keeling, C. D. *et al.* Atmospheric CO2 and 13CO2 exchange with the terrestrial biosphere and oceans from 1978 to 2000: observations and carbon cycle implications. in *A History of Atmospheric CO2 and its effects on Plants, Animals, and Ecosystems* (eds. Ehleringer, J. R., Cerling, T. E. & Dearing, M. D.) 83–113 (Springer Verlag, 2005).

57. Leroux, B. G., Lei, X. & Breslow, N. Estimation of Disease Rates in Small Areas: A new Mixed Model for Spatial Dependence. in *Statistical Models in Epidemiology,*

the Environment and Clinical Trials (eds. Halloran, M. & Berry, D.) 179–191 (Springer-Verlag, 2000). doi:10.1007/978-1-4612-1284-3_4.

58. Lee, D. CARBayes: An R package for Bayesian spatial modeling with conditional autoregressive priors. *J. Stat. Softw.* **55**, 1–24 (2013).

59. Gonzalez, A. *et al.* Scaling-up biodiversity-ecosystem functioning research. *Ecol. Lett.* **15**, ele.13456 (2020).

60. R Core Team. R: A Language and Environment for Statistical Computing. (2020).

Data availability

Data supporting the findings of this study are available in the following open repositories. CAMS: https://ads.atmosphere.copernicus.eu/cdsapp#!/dataset/cams-global-greenhouse-gas-inversion

CarboScope: http://www.bgc-jena.mpg.de/CarboScope/

Atmospheric CO_2 concentration: https://scrippsco2.ucsd.edu/data/atmospheric_co2/

Data from the TRENDY ensembles can be provided upon request from http://globalcarbonbudget.data.org/index.html. Data to reproduce Figures 1 and 2 are provided as Source Data. Code and data to perform the statistical analyses, calculations and figures is publicly available at Figshare: https://doi.org/10.6084/m9.figshare.17081717.v5.

Code availability

Code and data to perform the statistical analyses, calculations and figures is publicly available at Figshare: https://doi.org/10.6084/m9.figshare.17081717.v5.

Acknowledgements

This research was funded by the Spanish Government project PID2019-110521GB-I00, the Fundación Ramón Areces project CIVP20A6621, the Catalan government project SGR2017-1005, and the European Research Council project ERCSyG-2013-610028 IMBALANCE-P. M.F-M. was supported by a postdoctoral fellowship of the Research Foundation-Flanders (FWO) and is now supported by a fellowship from ”la Caixa”

Foundation (ID 100010434), code: LCF/BQ/PI21/11830010. We acknowledge the Scripps CO_2 program for providing the records of atmospheric CO_2.

Author contribution statement

MFM, JP, and IAJ planned and designed the research. FC, CR, SS, PF, VA, DG, AKJ, DLL and PCM provided the data. MFM analysed the data. All authors contributed substantially to the writing of the manuscript.

Author information statement

The authors declare no competing interest. Correspondence and requests for materials should be addressed to: Marcos Fernández-Martínez: m.fernandez@creaf.uab.cat